ORIGINAL PAPER

Stabilizing factors of the molecular structure in silicon-based peptidomimetics in gas-phase and water solution. Assessment of the correlation between different descriptors of hydrogen bond strength

María Pilar Gema Rodríguez Ortega · Manuel Montejo · Juan Jesús López González

Abstract The use of DFT (B3LYP and M06L) and *ab initio* (MP2) computational methods allowed us to perform a thorough conformational study of N-[dihydroxy (methyl)silyl]methylformamide (DHSF) and 3-[dihydroxy (methyl) silyl] propanamide (DHSP), that could be considered simplified models of the environment of the silanediol group in silicon gem-diols that have proven efficiency as protease inhibitors. We have found a total of 13 molecular conformations that represent minima in the potential energy surfaces of DHSF (six conformers) and DHSP (seven conformers). The key feature in their molecular structure is the occurrence of intramolecular hydrogen bonding between the hydroxyl and aminocarbonyl groups. We have estimated the strength of each individual hydrogen bond in the mentioned species using the descriptors proposed by three different methodologies, i.e., the quantum theory of atoms in molecules (QTAIM), the natural bond orbitals population analysis (NBO), and the so-called empirical Rozenberg's enthalpy-distance relationship. We have found a good correlation among the calculated values for the different descriptors within the whole set of conformers in the molecular systems in this study. We have also discussed the predicted order of stabilities of the different conformers of each species in terms of the so-called ring anomeric effect (RAE) and generalized anomeric effect (GAE). Finally, we also analyzed the discrepancies found in the order of stability when going from the isolated molecule approximation to water solution (PCM).

Introduction

Silanediol group has been found to have relevant pharmaceutical applications [1]. Indeed, peptidomimetics containing the silanediol group (silicon bioisosteres) have proven biological activity as inhibitors of metallo and aspartic proteases [2, 3]. The inhibition is supposed to occur after the quelation of the metal center *via* the formation of a tetrahedral *gem*-diol intermediate. The ability of the silanediol group to retain its tetrahedral structure [2], contrasting its carbon analogue that readily undergo dehydration, has motivated the development of molecular mimics of formerly known inhibitors where unstable carbons (in reaction intermediates and transition states) are replaced by silicon atoms. However, this advantageous characteristic is blurred by the propensity of gem-silanediols toward self-condensation, giving oligomers (siloxanes) and chains [4]. This fact prevents the use of alkylgem-silanediols as inhibitors.

The conformational properties of geminal silanediols and their ability to intramolecular hydrogen bonding could largely reduce their tendency toward policondensation and, hence, their polimerization [5]. Steric effects are also responsible for the increasing stability of the silanediol group. Specifically, the above mentioned silicon bioisosteres can be divided into groups attending to the environment of the $Si(OH)_2$ functionality, i.e., the aminocarbonyl group can be in β or γ position with respect to the silicon atom.

M. P. G. Rodríguez Ortega · M. Montejo · J. J. López González (✉)
Department of Physical and Analytical Chemistry. Experimental Sciences Faculty, University of Jaén, Campus "Las Lagunillas", 23071 Jaén, Spain
e-mail: jjlopez@ujaen.es

In this work, we have studied the molecular and electronic structure of N-[dihydroxy(methyl)silyl]methylformamide (DHSF) and 3-[dihydroxy(methyl)silyl] propanamide (DHSP) (Fig. 1), species that mimic the environment of the gem-silanediol functionality in biological active silanediols.

Several theoretical studies focused on such interactions between metal binding groups (MBGs) and metalloproteases have been reported [6–9], but few of them used silanediol functionality as MBG. Therefore, the results obtained in the present work can be useful for the understanding of the chemistry of these compounds, which, in a second stage, will be of interest for the study of the interaction mechanisms of this sort of species with metallic centers.

The potential energy surfaces (PES) of the above mentioned silanediols, have been thoroughly analyzed. Intramolecular hydrogen bonding in the set of conformers studied for each system has been characterized using the AIM theory [10], NBO population analyses [11] and the Rozenberg's empirical enthalpy equation [12]. Additionally, NBO population analyses have been used to evaluate the conformational properties of the set of conformers considering the stabilization that arises from the ring anomeric effect (RAE) as well as the generalized anomeric effect (GAE). This analysis has provided a better insight on the most important stabilizing factors in this sort of compound. Finally, DFT calculations performed in water solution (PCM) helped assess the effects that the media induce in both, molecular structure and stability of the systems studied.

Theoretical methods

Ab initio and DFT calculations were performed using the Gaussian 09 [13] suite of programs. All stationary points were fully optimized and characterized by harmonic vibrational frequency calculations using the B3LYP hybrid density functional [14, 15], the M06L pure density functional [16] and the second order Möller-Plesset perturbation theory [17] in conjunction with the cc-pVDZ [18], cc-pVTZ [18] and aug-cc-pVTZ [19] basis sets (these last two only in the case of DFT calculations). B3LYP is considered as standard model chemistry for many applications and has proven its efficiency for the study of thermochemical and spectroscopies properties in
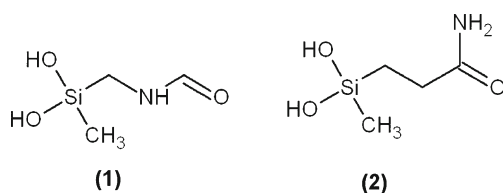
a wide range of molecular systems. The M06L functional was also chosen to study the above mentioned systems since it has been reported to have the best overall performance for the study of organometallic and non-covalent interactions [20, 21]. However, since hydrogen-bonded systems are governed not only by the dominant electrostatic component but also by dispersion interactions, they are commonly poorly described for many DFT functionals, which fail to describe dispersion interactions accurately. In fact, semilocal and local density functionals cannot describe the long-range performance of the van der Waals interactions (missing the correct attractive $1/R^6$ behavior) leaving the interaction solely to the Coulomb terms. Thus, the DFT-D3 program of Grimme et al. [22] was used to correct the calculated B3LYP/cc-pVDZ energies of the systems into study. Since pure M06L functional already behave well for this kind of interactions [23], the dispersion correction of the calculated E_0 energies at this level was discarded.

Solvent calculations were carried out according to the polarizable continuum model (PCM) [24] as implemented in Gaussian 09.

Natural bond orbital (NBO) [11] calculations were accomplished using the program NBO v3.1 [25] as implemented in Gaussian 09. For all molecules, AIM calculations based on Bader's theory [10] were performed using AIM2000 program [26, 27].

Results and discussion

Theoretical conformational analysis and molecular structure of DHSF and DHSP molecule

Gas-phase study

Conformational searching was carried out performing a simultaneous fully relaxed scan (B3LYP/6-31+G*) of the ψC_{14}-N_{13}-C_4-Si and ψN_{13}-C_4-Si-C_5 dihedral angles (DHSF), and the ψC_4-C_5-C_6-N and ψSi-C_4-C_5-C_6 dihedral angles (DHSP), which allows obtaining their corresponding potential energy surfaces (Figs. S1 and S2, respectively) concerning the arrangement of the hydroxyl groups and the side chains. The molecular conformations with minor relative energies were isolated and then optimized at the above mentioned level of theory. The subsequent computation of the harmonic vibrational frequencies revealed the existence of six possible local minima (no imaginary frequencies) for the DHSF (shown in Fig. 2) and seven conformations (Fig. 3) for DHSP. In most of the isolated structures, an intramolecular hydrogen bond between the aminocarbonyl group and, at least, one of the -OH groups is established. Table 1 reports all the stationary points characterized as real minima on the PES of the two systems in this study, their symmetry point

Fig. 1 Molecular schemes of (1) N-[dihydroxy(methyl)silyl]methyl} formamide (DHSF) and (2) 3-[dihydroxy(methyl)silyl]propanamide (DHSP)

groups and relative energies (ΔE_0 in kcal mol^{-1}). As can be seen in Table 1, for DHSF, the relative energies (ΔE_0) calculated with the B3LYP, M06L and MP2 methods, in conjunction with the cc-pVDZ, cc-pVTZ and aug-cc-pVTZ basis sets (these last two only for DFT calculations), show the same trend. Both the *ab initio*/ MP2 energy differences between conformers and the predicted order of stability, agree with DFT calculations, yielding comparable results. Besides, the inclusion of dispersion effects in the calculated B3LYP/cc-pVDZ E_0 energies yields values even closer to the MP2 results. Remarkably, the energy difference between conformers decrease as the size of the basis set increases.

For DHSP, the relative energies (ΔE_0) calculated for the set of conformers with the B3LYP, M06L and MP2 methods, in conjunction with the cc-pVDZ, cc-pVTZ and aug-cc-pVTZ (except in the use of MP2) basis sets, show a similar trend. In general, DFT calculations match *ab initio* results. The dispersion corrected B3LYP/cc-pVDZ energies are also very close to the values calculated at the MP2 level. Albeit there are subtle discrepancies in the predicted stability orders depending on the method, being the energy differences in these cases less than 0.5 kcal mol^{-1}. This is for example the case for conformer II, which is the most stable structure according to M06L calculations but it is the second most stable conformer for B3LYP and MP2 calculations.

As expected, and confirmed from the ΔE_0 values reported in Table 1, for both systems, conformers which are characterized for the occurrence of intramolecular hydrogen bonds are more stable in gas phase than the remaining.

The main geometrical parameters calculated for the conformers of the DHSF and DHSP at the MP2/cc-pVDZ level of theory are collected in Tables S1 and S2. Indeed, and unless otherwise stated, we will refer to MP2/cc-pVDZ bond lengths and energies all along this discussion.

Focusing on DHSF, its global energy minimum (conformer I) correspond to a C_s structure, where the carbonyl group establish a tricentric H-bond with the two hydroxyl groups of the molecule (217.7 pm), resulting in a seven-membered bicycle.

Conformer II and III (*ca.*1.5 kcal mol^{-1} higher in energy than conformer I) are arranged in a six-membered ring through the formation of an H-bond between the carbonyl group and the -O_2H_6 (189.9 pm) and -O_3H_7 (209.4 pm) hydroxyl groups, respectively. The main structural difference between conformers II and III is related to the *axial/equatorial* position of the methyl and hydroxyl groups with respect to the *pseudo*-cycle. Structure of conformer II is the one that is expected to be favored considering the anomeric effect in a ring, being the -O_3H_7 hydroxyl group disposed in *axial* arrangement with respect to the endocyclic heteroatom. In addition, the -OH groups in conformer II are also arranged according to the most stable geometry considering the generalized anomeric effect in gem-silanediols [28–30]. Finally, in conformers IV, V and VI, no intramolecular H-bonds are established.

Considering DHSP molecule, global energy minimum (conformer I) is arranged in a seven-membered ring, where one hydroxyl group is bound to the carbonyl group *via*
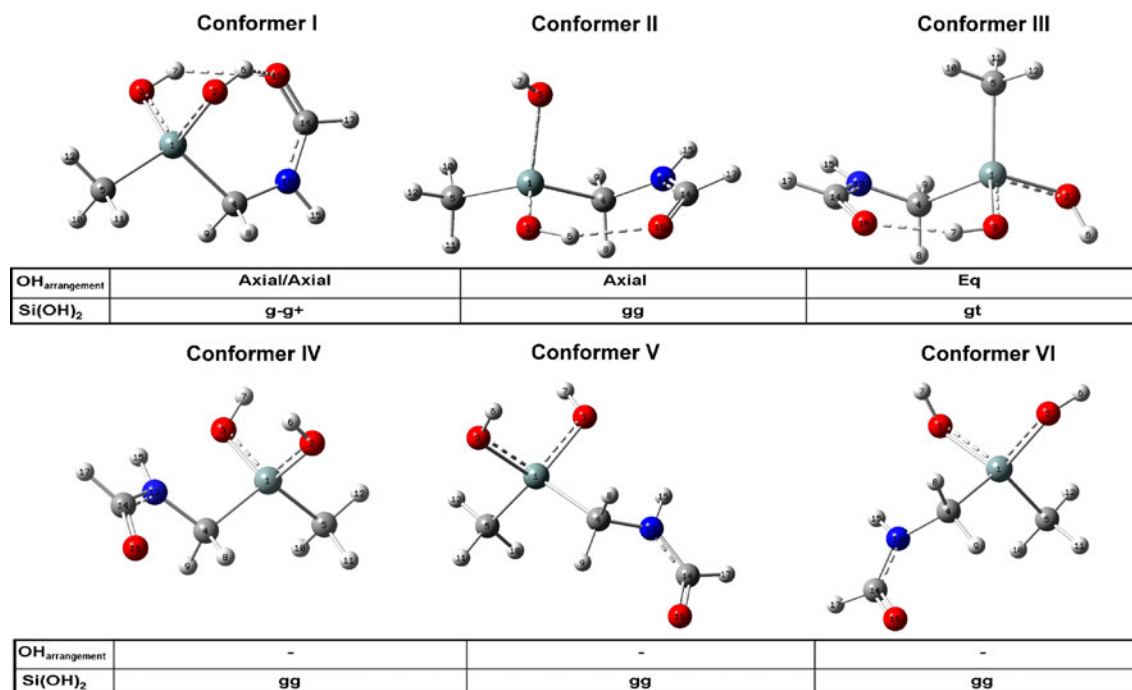

$OH_{arrangement}$	**Axial/Axial**	**Axial**	**Eq**
$Si(OH)_2$	g-g+	gg	gt

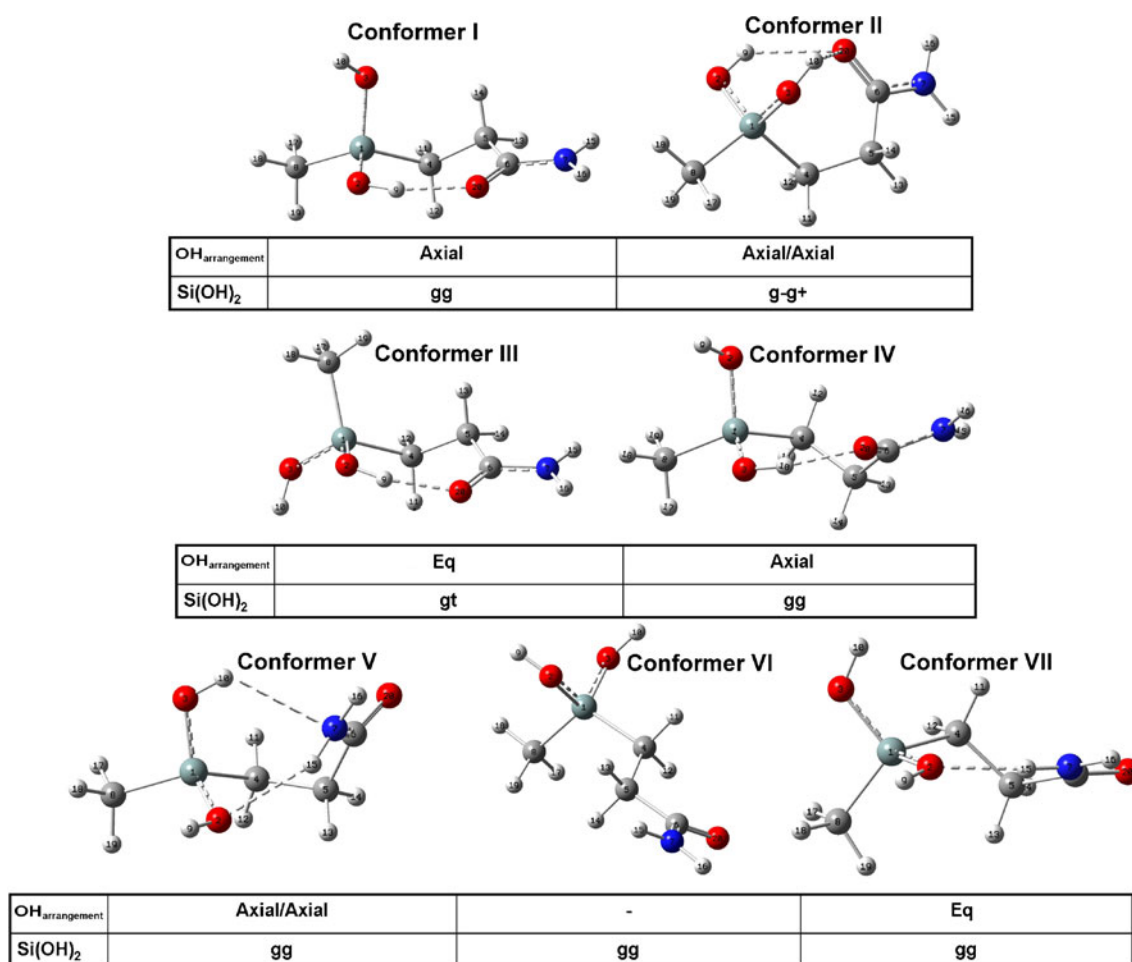| $OH_{arrangement}$	-	-	-
$Si(OH)_2$	gg	gg	gg

Fig. 2 DHSF's set of conformers

Fig. 3 DHSP's set of conformers

intramolecular hydrogen bonding (192.4 pm). Conformer II is characterized for the occurrence of two intramolecular hydrogen bonds, being the carbonyl group simultaneously interacting with both -OH groups (217.2 pm and 227.8 pm). Conformers III and IV form a seven-membered cycle through H-bond between one hydroxyl group and the carbonyl group. The main difference between these conformers lay on the relative position of methyl and hydroxyl groups with respect to the ring plane. For conformer III, -OH group is arranged in *equatorial* position whereas for conformer IV it is in *axial* (geometry most favored by RAE).

In conformer V, two intramolecular hydrogen bonds are established between the amino group and both hydroxyl groups, being the former acting as proton donor and as acceptor simultaneously. Conformer VII establishes an H-bond between one of the hydroxyl groups and the amino group. The *exo* -OH group is disposed in *equatorial* arrangement respect to the resulting ring plane. Finally, conformer VI is characterized by the non-occurrence of intramolecular hydrogen bond.

In order to justify the stability order predicted by gas-phase calculations, three different stabilizing effects taking place in

the set of conformers of both systems were analyzed: (a) the strength of the intramolecular hydrogen bonds, (b) the ring anomeric effect (RAE) and (c) the generalized anomeric effect (GAE).

(a)   Intramolecular hydrogen bonding

It is known that the stabilization of *quasi*-cyclic structures by intramolecular hydrogen bonds (interaction which is considered as a particular case of hydrogen bonding) can possibly be accompanied by certain conjugation effects [31].

Unlike intermolecular hydrogen bonds, the energy of intramolecular interactions cannot be easily calculated. Several theoretical approaches have been proposed to quantify such interactions [32–34].

Among the vast amount of descriptors used to characterize hydrogen bonds, geometric criteria (i.e., hydrogen bond distances and angles) are often applied as a standard approach to study H-bondings and calculate their energies. This has led to the development of empirical equations, where both stretching vibration shift and H-bond length are used to quantify H-bond strength [12,

Table 1 Effect of the increasing basis set size on the relative energies (ΔE_0, in kcal mol^{-1}) for DHSF and DHSP

Stationary point	$\Delta E_0{}^a$ (kcal mol^{-1})							
	B3LYP				M06L			MP2
	cc-pVDZ	cc-pVDZ$_{DC}{}^b$	cc-pVTZ	aug-cc-pVTZ	cc-pVDZ	cc-pVTZ	aug-cc-pVTZ	cc-pVDZ
DHSF								
I (C_S)	0.00	0.00	0.00	0.00	0.00	0.00	0.00	0.00
II (C_1)	0.83	1.19	0.56	0.33	1.95	1.66	1.37	1.32
III (C_1)	1.43	1.55	0.97	0.69	1.30	1.40	0.90	1.33
IV (C_1)	4.17	5.00	3.09	2.62	5.33	5.18	5.06	4.72
V (C_1)	4.28	5.08	3.20	2.69	5.39	5.04	4.39	4.75
VI (C_1)	5.07	5.86	3.77	3.22	6.35	5.81	5.38	5.60
DHSP								
I (C_1)	0.00	0.00	0.00	0.00	0.32	0.04	0.26	0.00
II (C_1)	0.98	0.46	0.94	0.99	0.00	0.00	0.00	0.30
III (C_1)	2.06	2.12	1.41	1.27	1.62	1.83	1.69	1.85
IV (C_1)	1.98	1.88	1.84	1.90	2.90	2.18	2.22	1.96
V (C_1)	4.07	3.19	4.01	4.03	3.82	3.58	3.40	2.63
VI (C_1)	5.94	6.65	4.04	3.48	6.33	4.97	4.77	5.89
VII (C_1)	5.51	5.44	4.75	4.40	6.03	5.58	5.23	5.47

[a] Stand for zero-point corrected relative energy

[b] Subscript DC denote the E_0 relative energies corrected by dispersion effects

35]. One example of these is the Rozenberg's enthalpy-distance relationship [12] that is used to determine the enthalpy of the hydrogen bond (ΔH) from the theoretical and experimental values of the hydrogen bond distance (r):

$$-\Delta H(kcal/mol) = 0.0321 \, r^{-3.05} (\text{with r in nm})$$

Besides empirical approximations, both the natural bond orbital theory (NBO) and the quantum theory of atoms in molecules (QTAIM) have been largely used to detect and characterize hydrogen bonding, from a strictly theoretical point of view.

In the natural bond orbital (NBO) approach, a hydrogen bond is interpreted as an interaction between a lone pair of the charge donor atom and the unoccupied antibonding orbital of the XH bond (σ^* XH). The NBO charge transfer orbital interaction energy ($\Delta E^{(2)}_{\sigma\sigma^*}$) is given by the formula

$$\Delta E^{(2)}_{\sigma\sigma^*} = -2 \frac{<\sigma|\hat{F}|\sigma*>^2}{e_\sigma - e_{\sigma*}},$$

where $\hat{F}$ is the Fock operator and e_σ and $e_{\sigma*}$ are NBO orbital energies [11]. This interaction energy could be used as a measure of the hydrogen bond strength.

As concerns the AIM theory, Koch and Popelier established a series of criteria that should be taken into account for a proper analysis of an H-bond [36]. Thus, there must be a consistent topology (i.e., the existence of a bond critical point, BCP, connecting the two nuclei, an interatomic surface or zero-flux surface and a bond path between them) for each hydrogen bond. At the BCP the value of $\rho(r)$ must lie within the range [0.002, 0.04] au, and the value of the *Laplacian* of the electron density, $\nabla^2\rho(r)$, must lie within the range [0.6, 0.08] au, so that any hydrogen bonding is interpreted as a closed-shell interaction ($\nabla^2\rho(r) > 0$ at the BCP) in the AIM theory. These three criteria are considered as the most determinant factors to confirm the presence of a hydrogen bond.

Table 2 shows a summary of calculated (MP2/cc-pVDZ) parameters used, in this work, to characterize the strength of the hydrogen bonds appearing in the set of conformers of DHSF. Likewise, in Table 3 are summarized the considered parameters to analyze intramolecular hydrogen bonds in conformers of DHSP.

For both systems, the enthalpy values calculated are within the expected range for an intramolecular hydrogen bond. Remarkably, the value of $\nabla^2\rho(r)$ in the BCPs is correlated with both ΔH values and NBO interaction energies, as shown in Fig. 4 (where the parameters of the nine conformers of the two species into study that present intramolecular hydrogen bonds have been taken into account).

As shown in Table 2, for DHSF, hydrogen bond in conformer II is found to be the strongest. However, the higher enthalpy is

Table 2 Intramolecular hydrogen bond descriptors for DHSF

		MP2/cc-pVDZ		
		I	II	III
	r H-bond[a]	217.7	189.9	209.4
		217.7		
NBO delocalizations (kcal mol^{-1})	LP(1,2) Y→σ*XH[b]	1.10	6.13	2.34
		0.85	5.62	1.70
		1.10	–	–
		0.85	–	–
AIM parameters (a.u)	$\rho(r)$	0.017831	0.026938	0.019909
		0.017831		
	$\nabla^2\rho(r)$	0.064320	0.104860	0.072676
		0.064320		
Rozenberg's enthalpy (kcal mol^{-1})[c]	-ΔH	3.35	5.09	3.77
		3.35		

[a] Bond distances in pm

[b] NBO interactions of intramolecular hydrogen bonding in conformer I (LP (1) O_{16}→σ* O_2H_6; LP (2) O_{16}→σ*O_2H_6; LP (1) O_{16}→σ* O_3H_7; LP (2) O_{16}→σ* O_3H_7) in conformer II (LP (1) O_{16}→σ* O_2H_6; LP (2) O_{16}→σ*O_2H_6) and in conformer III (LP (1) O_{16}→σ* O_3H_7; LP (2) O_{16}→σ* O_3H_7)

[c] Enthalpy of the intramolecular hydrogen bond calculated using the empiric equation of Rozenberg

conformers with more than one H-bond, such as conformer II (6.30 kcal mol^{-1}) and conformer V (6.14 kcal mol^{-1}).

As mentioned above, conformers I, II and III of DHSF are calculated to be lower in energy than conformers IV, V and VI. Thus, the stability order inferred considering the total amount of energy released when the H-bond is established, is consistent with the predicted order of stability (I<II<III) computed at the aforementioned level of theory for this system. On the contrary, in the case of DHSP, the stability order inferred only considering the energy of the intramolecular H-bond (II<V<IV<VII<I<III<VI), does not match with the order of stability set up by the ΔE_0 values computed at the MP2 level. This fact may be caused by the combined effect of the stabilization that arises from H-bond formation and other destabilizing interactions (e.g., steric effects) that may appear as a result of the side chain folding.

(b) Ring anomeric effect (RAE)

One of the main principles of the conformational analysis is that the substituents of a cyclohexane ring tend to adopt *equatorial* disposition rather than *axial* arrangement, mainly due to steric reasons [37–41]. Nevertheless, it has been seen that polar substituents with lone electron pairs (groups such as OMe, OAc, Cl, etc., known as anomeric substituents) show a preference to adopt the *axial* position. Several explanations have been proposed to explain the origin of the ring anomeric effect [37–41]. According to the electrostatic theory, this tendency to adopt *axial* positions in a six-membered ring is the result of destabilizing interactions between the dipole

calculated for conformer I (with two H-bonds), for which total enthalpy reaches a value of 6.70 kcal mol^{-1}. Similarly, the strongest individual hydrogen bond is found in conformer VII of DHSP. Nonetheless, the highest enthalpy is calculated for those

Table 3 Intramolecular hydrogen bond descriptors for DHSP

		MP2/cc-pVDZ						
		I	II	III	IV	V	VI	VII
	r H-bond[a]	192.4	217.2	206.1	187.4	222.1	–	191.9
			227.8			226.4		
NBO delocalizations (kcal mol^{-1})	LP(1,2)Y→σ*XH[b]	5.51	1.51	2.99	4.67	5.23	–	11.23
		4.66	0.80	1.81	9.43	1.62	–	1.16
		–	1.03	–	–	1.86	–	–
		–	–	–	–	–	–	–
AIM parameters (a.u)	$\rho(r)$	0.025038	0.016788	0.020211	0.028665	0.018067	–	0.024864
			0.014592			0.014898		
	$\nabla^2\rho(r)$	0.097936	0.060380	0.065956	0.109696	0.053410	–	0.103604
			0.051796			0.049406		
Rozenberg's enthalpy(kcal mol^{-1})[c]	-ΔH	4.89	3.38	3.96	5.30	3.16	–	4.93
			2.92			2.98		

[a] Bond distances in pm

[b] NBO interactions of intramolecular hydrogen bonding in conformer I (LP(1) O_{20}→σ*O_2H_9; LP(2) O_{20}→σ*O_2H_9), in conformer II (LP(1) O_{20}→σ*O_2H_9; LP(2) O_{20}→σ*O_2H_9; LP(2) O_{20}→σ*O_3H_{10}), in conformer III (LP(1) O_{20}→σ*O_2H_9; LP(2) O_{20}→σ*O_2H_9), in conformer IV (LP(1) O_{20}→σ*O_3H_{10}; LP(2) O_{20}→σ*O_3H_{10}), in conformer V (LP (1) O_2→σ*N_7H_{15}; LP (2) O_2→σ*N_7H_{15}; LP(1) N_7→σ*O_3H_{10}) and in conformer VII (LP (1) O_2→σ*N_7H_{15}; LP (2) O_2→σ*N_7H_{15})

[c] Enthalpy of the intramolecular hydrogen bond calculated using the empiric equation of Rozenberg

Fig. 4 Correlation between the values of the *Laplacian* of electron density, NBO charge transfer orbital interaction energies (kcal mol^{-1}) and Rozenberg's enthalpies (kcal mol^{-1}) of all the individual intramolecular hydrogen bonds in DHSF (triangle/blue) and DHSP (dot/red)
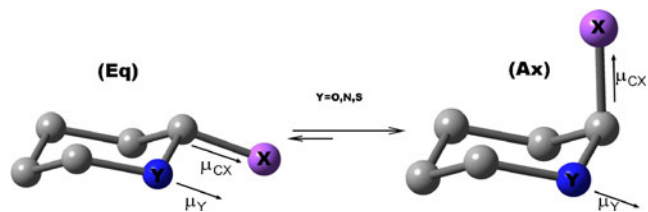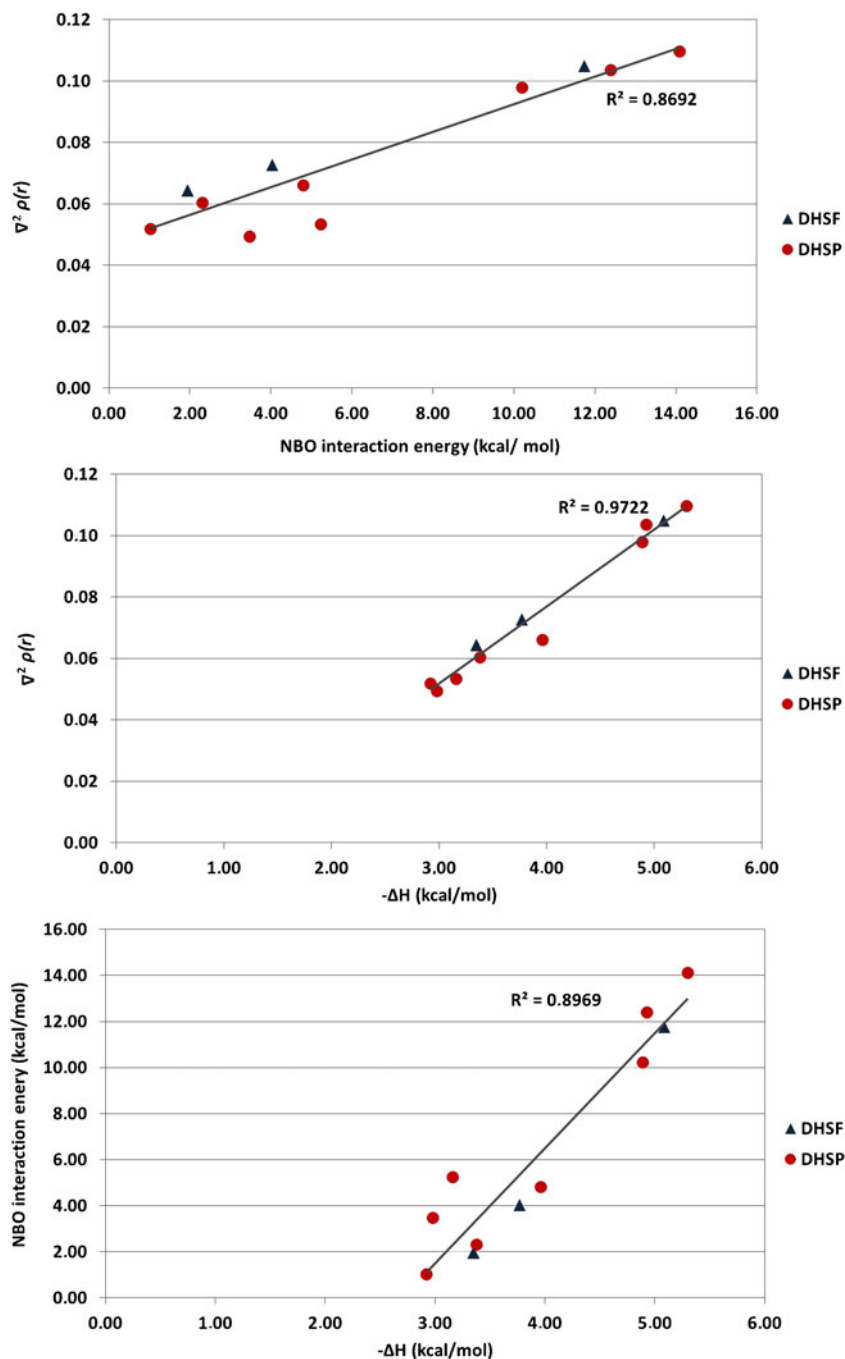

Fig. 5 Schematic representation of dipole-dipole interactions of polar bonds in a hypothetical substituted heterocyclic compound, where X being any polar substituents with lone electron pairs (such as OMe, OH, Cl, etc.). *Axial/equatorial* conformational preference

moments of the polar bonds involved in the anomeric center (see Fig. 5). This dipole-dipole interaction is diminished when the polar substituents adopt *axial* disposition.

Moreover, bearing in mind the hyperconjugative model, the stabilization of the *axial* conformer is attributed to the delocalization of the antiperiplanar lone pair orbital on the endocyclic heteroatom (Y) to the σ* antibonding orbital of the C-X bond. This interaction produces the lengthening of the C-X bond by electron transfer to its σ* antibonding orbital whereas the C-Y is contracted by

increasing its double-bond character. Besides, the Y-C-X bond angle is opened as a consequence of the resulting sp^2 character on the anomeric center.

Considering DHSF molecule, for conformer II (see Table S1), which adopt the favored ring anomeric geometry, the Si-O_2 distance (endocyclic heteroatom) is much shorter than Si-O_3 bond length (anomeric substituent), being the former 167.7 pm whereas the latter takes a value of 169.4 pm. The theoretical value of OSiO bond angle (113.8°) is far away from the classical value for tetrahedral silicon. Nonetheless, for conformer III, which is the geometrical counterpart of conformer II, this angle is calculated to be 104.6° which, indeed, is smaller than the expected value for tetrahedral silicon. In addition, the Si-O_3 bond length (endocyclic heteroatom) is not as small as it would be expected for a system where the ring anomeric effect is structurally promoted.

Due to molecular symmetry, both Si-O distances in conformer I have the same value. In addition, both hydroxyl groups are disposed in *axial* arrangement respect to the bicycle plane, being the charge transfer equally favored from both oxygen atoms.

In the case of DHSP, the values of bond distances and angles in conformer I (reported in Table S2) are consistent with the occurrence of the RAE. For example, Si-O_2 bond distance is much shorter than Si-O_3 and, besides, the OSiO bond angle is larger than the value expected for sp^3 silicon (112.7°). The same goes for conformer III, although, in this case, the value of the OSiO bond angle (105.1°) is smaller than that expected in a sp^3 center, an effect that could be caused by the *gauche-trans* arrangement of hydroxyl groups in this conformer. The incidence of the RAE is also observed in the values of the calculated geometrical parameters for conformer IV and VII. On the other hand, the calculated Si-O bond distances in conformer V (171.2 pm SiO_2, 168.7 SiO_3) do not fit those expected for a system favored by the ring anomeric effect. This discrepancy could be the result of the lifting balance of hyperconjugative interactions derived from the fact that both hydroxyl groups are involved in hydrogen bonds.

Tables 4 and 5 outline the $\Delta E^{(2)}_{\sigma\sigma*}$ values of the charge transfer taking place from the lone pairs of both oxygen atoms used to evaluate the ring and generalized anomeric effects in the set of conformers of both systems, computed at the MP2/cc-pVDZ level.

For DHSF, the highest total contribution to the ring anomeric effect is calculated for conformer I, in which both hydroxyl groups are disposed in *axial* arrangement with respect to the bicycle plane. The value of the RAE of conformer II is *ca.* 4.2 kcal mol^{-1} higher than the calculated value for conformer III. This is in accordance with the *axial/equatorial* disposition of methyl and hydroxyl groups in this pair of conformers.

Table 4 NBO data used to evaluate ring and generalized anomeric effects in the set of DHSF conformers

Interaction	MP2/cc-pVDZ					
	$E^{(2)}_{\sigma\sigma*}$ (kcal mol^{-1})					
	I	II	III	IV	V	VI
LP (1) $O_2 \rightarrow \sigma*$ SiO_3	**2.26**	**1.25**	4.31	1.00	1.80	0.78
LP (1) $O_2 \rightarrow \sigma*$ SiC_4	2.24	3.64	1.73	3.21	2.56	3.04
LP (1) $O_2 \rightarrow \sigma*$ SiC_5	2.55	2.13	–	2.59	2.65	3.56
LP (2) $O_2 \rightarrow \sigma*$ SiO_3	**13.46**	**17.35**	3.02	15.65	14.18	16.04
LP (2) $O_2 \rightarrow \sigma*$ SiC_4	9.14	6.49	3.36	5.35	7.05	–
LP (2) $O_2 \rightarrow \sigma*$ SiC_5	–	0.73	9.57	–	–	5.09
LP (1) $O_3 \rightarrow \sigma*$ SiO_2	**2.26**	3.10	**4.16**	1.61	0.89	2.43
LP (1) $O_3 \rightarrow \sigma*$ SiC_4	2.24	3.40	1.86	3.12	2.94	1.52
LP (1) $O_3 \rightarrow \sigma*$ SiC_5	2.55	1.49	1.84	2.23	2.87	2.71
LP (2) $O_3 \rightarrow \sigma*$ SiO_2	**13.46**	9.92	**10.26**	12.64	14.39	10.83
LP (2) $O_3 \rightarrow \sigma*$ SiC_4	9.14	–	–	–	–	–
LP (2) $O_3 \rightarrow \sigma*$ SiC_5	–	9.29	8.94	6.78	5.34	7.97
$\sum$RAE[a]	31.44	18.60	14.42	–	–	–
$\sum$GAE[b]	59.30	58.79	49.05	54.18	54.67	53.97

[a] Stand for the ring anomeric effect. The individual contribution to the RAE of each conformer according to the position (*endo* or anomeric substituent) of O_2 and O_3 oxygen atoms in the *pseudo*-cycle are shown in bold

[b] Stand for the generalized anomeric effect

Focusing on the conformers of DHSP, the highest value of $\sum$RAE is found in conformer V as it has two anomeric substituents properly oriented (*axial/axial*) with respect to the ring plane. The same goes for conformer II (also with both –OH groups in *axial/axial* arrangement), which is calculated to have the second highest value of $\sum$RAE. The value of $\sum$RAE for conformer IV is much higher than that of conformer III, as expected since the geometry of the latter is not favored by ring anomeric effect. Finally, conformer I (-OH *axial*) is more favored by RAE than conformer VII (-OH *equatorial*) as shown in Table 5.

Noticeably, the calculated values of RAE for conformers of DHSF are also consistent with the predicted stability of the considered set of conformers from the E_0 energies. However, the use of the magnitude of $\sum$RAE to set up the stability order among the set of conformers (V<II<I<IV<VII<III<VI) for DHSP also yields a different trend than that obtained considering the values of ΔE_0 at the MP2/cc-pVDZ level.

(c) Generalized anomeric effect (GAE)

Considering a structural motif like $\alpha-\beta-\gamma-\delta$, where α is an electronegative atom and δ has at least one lone electron pair, the hyperconjugative model explains the generalized anomeric effect as an electron donation from

Table 5 NBO data used to evaluate ring and generalized anomeric effects in the set of DHSP conformers

Interaction	MP2/cc-pVDZ						
	$E^{(2)}{}_{\sigma\sigma*}$ (kcal mol^{-1})						
	I	II	III	IV	V	VI	VII
LP (1) O$_2$→σ* SiO$_3$	**0.88**	**1.43**	**3.89**	2.48	**1.48**	1.45	–
LP (1) O$_2$→σ* SiC$_4$	3.87	2.85	2.41	2.97	2.88	2.92	2.39
LP (1) O$_2$→σ* SiC$_8$	2.07	2.39	1.20	2.31	2.26	2.49	3.32
LP (2) O$_2$→σ* SiO$_3$	**18.02**	**15.09**	–	11.27	**12.63**	13.63	**14.16**
LP (2) O$_2$→σ* SiC$_4$	5.16	7.09	8.29	–	–	–	0.51
LP (2) O$_2$→σ* SiC$_8$	0.95	–	9.84	8.50	5.78	6.51	4.26
LP (1) O$_3$→σ* SiO$_2$	2.07	**2.30**	3.64	**1.68**	**1.44**	1.17	1.27
LP (1) O$_3$→σ* SiC$_4$	3.17	1.78	1.94	2.97	3.08	2.94	3.13
LP (1) O$_3$→σ* SiC$_8$	1.98	2.38	–	2.31	2.29	2.64	2.69
LP (2) O$_3$→σ* SiO$_2$	11.52	**11.82**	4.99	**15.85**	**15.88**	15.05	15.55
LP (2) O$_3$→σ* SiC$_4$	–	8.74	2.00	7.61	6.70	5.83	5.95
LP (2) O$_3$→σ* SiC$_8$	7.71	–	9.86	–	–	–	–
∑RAE[a]	18.90	30.64	3.89	17.53	31.43	–	14.16
∑GAE[b]	57.4	55.87	48.06	57.95	54.42	54.63	53.23

[a] Stand for the ring anomeric effect. The individual contribution to the RAE of each conformer according to the position (*endo* or anomeric substituent) of O$_2$ and O$_3$ oxygen atoms in the *pseudo*-cycle are shown in bold

[b] Stand for the generalized anomeric effect

δ atom to the σ* antibonding orbital of the γ−β bond, causing the shortening of the γ−δ bond and the lengthening of the adjacent γ−β bond [37–41]. As was previously stated for small alkylsilanediols [28–30], the stabilizing generalized anomeric effect in gem-silanediols is favored when -OH groups are oriented in *gauche*. The influence of the hyperconjugative effects in the calculated geometries was also studied using NBO population analyses for the set of conformers.

As concerns DHSF, conformer III present the lowest value of ∑GAE (see Table 4), as expected, since their hydroxyl groups are disposed in *gauche-trans* orientation. Consequently, the mentioned charge transfer came mostly from the O$_2$ oxygen atom (which is properly oriented), whereas in the remaining conformers it is coming from both hydroxyl groups.

For the set of conformers of this system, the total contribution to the ∑GAE is quite high and rather similar, except

for conformer III. However, although conformers I and II are those with the highest values of ∑GAE, the stability order considering this effect (I<II<V<IV<VI<III) does not match exactly the order predicted by the E$_0$ energies. Other stereoelectronics and sterics effects may be responsible for the predicted order of stability computed in gas-phase. In this case, the strength of the intramolecular hydrogen bonding and the *axial/equatorial* disposition of substituents with respect to the ring plane may contribute further to the computed E$_0$ values in gas-phase.

Considering DHSP, only for conformer VI (no H-bonds) both Si-O and Si-C lengths (reported in Table S2) are similar. This is expected in systems with *gg* arrangement of hydroxyl groups. The remaining conformers show large discrepancies in the mentioned geometrical parameters, although the -OH groups are also disposed in *gg* arrangement. This could be caused by the enhancement of hyperconjugative interactions as a result of the intramolecular hydrogen bonding in these systems. Except for conformer III, the values of ∑GAE (see

Table 6 Compared geometries, dipole moments and relative energies for DHSF conformers in the isolated molecule approximation and in water solution, along with their solvation energies (E$_0{}^{sol}$)

Geometrical parameters	Gas-phase[a] (B3LYP/aug-ccpVTZ)					
	I	II	III	IV	V	VI
r H-bond	226.9	191.3	191.5	–	–	–
r SiO$_2$	165.5	164.5	165.9	165.9	165.8	165.9
r SiO$_3$	165.5	166.4	164.6	166.9	166.9	166.8
r SiC$_4$	191.6	191.0	191.5	188.8	188.8	188.6
r SiC$_5$	186.3	186.7	186.5	186.2	186.2	186.3
r C$_4$N$_{13}$	146.3	146.6	146.8	145.9	145.8	145.9
r N$_{13}$C$_{14}$	134.1	134.3	134.5	135.5	135.5	135.6
∠OSiO	114.6	112.5	108.1	111.0	112.1	111.6
μ (Debye)	4.78	3.72	4.15	4.28	4.56	4.55
ΔE$_0$ (kcal mol^{-1})	0.00	0.33	0.69	2.62	2.69	3.22
	Water solution[a] (PCM-B3LYP/aug-ccpVTZ)					
	I	II	III	IV	V	VI
r H-bond	222.0	186.0	182.4	–	–	–
r SiO$_2$	166.7	166.0	165.8	166.0	166.0	166.0
r SiO$_3$	166.7	166.1	166.0	166.2	166.0	166.2
r SiC$_4$	190.2	190.2	190.7	189.3	189.3	189.5
r SiC$_5$	186.2	186.6	186.4	186.5	186.5	186.5
r C$_4$N$_{13}$	146.2	146.6	146.7	146.0	146.0	146.0
r N$_{13}$C$_{14}$	133.1	133.0	133.0	133.9	133.9	134.0
∠OSiO	112.3	112.2	110.2	111.6	112.5	112.3
μ (Debye)	7.37	6.01	6.96	6.60	6.73	6.59
ΔE$_0$ (kcal mol^{-1})	7.74	2.02	1.98	0.20	0.06	0.00
E$_0{}^{sol}$ (kcal mol^{-1})	−11.84	−17.88	−18.28	−21.99	−22.20	−22.79

[a] Bond distances in pm

Table 5) within the set of conformers are alike.

Again, the stability order that can be concluded from the ∑GAE values (IV<I<II<VI<V<VII<III) does not follow the trend of the computed ΔE_0 values.

Contrasting DHSF, in the case of DHSP the strength of the hydrogen bonds (II<V<IV<VII<I<III<VI) and the magnitude of the RAE (V<II<I<IV<VII<III<VI) follow a rather similar tendency within the set of conformers. Nonetheless, as stated above, the stability order predicted considering the relative ΔE_0 energies by MP2/cc-pVDZ calculations under the isolated molecule approximation is different and may be due to the combined effect of all the stabilizing effects (i.e., H-bond formation, RAE, and GAE, among others) and destabilizing interactions (e.g., steric effects). The stabilization of each molecular conformation is due to the joint effect of stabilizing and destabilizing factors. The folding of the long side chain in this system is promoted by the establishment of intramolecular hydrogen bond (which is a stabilizing interaction). However, the energy lowering derived from the hydrogen bond formation could be compensated by other destabilizing interactions (mainly stereoelectronics effects) that may arise from the geometry adopted by the alkyl side chains when the H-bond is established. This could explain the differences between the stability order predicted considering ΔE_0 energies and the enthalpies of H-bonds, as well as the discrepancies found when RAE and GAE are evaluated.

Solvent calculations

The influence of the media on the molecular structure and stability of the DHSF and DHSP conformers was evaluated performing the geometrical optimization of the different molecular conformations in water solution using the PCM model (B3LYP/aug-cc-pVTZ).

The dipole moments and the main geometrical parameters in water solution (PCM) as well as the solvation energies (E_0^{sol}) calculated at the B3LYP/aug-cc-pVTZ level for all the conformers of the two systems in this study, along with their corresponding parameters calculated in gas-phase are collected in Tables 6 and 7. The most significant phase effects

Table 7 Compared geometries, dipole moments and relative energies for DHSP conformers in the isolated molecule approximation and in water solution, along with their solvation energies (E_0^{sol})

Geometrical parameters	Gas-phase[a] (B3LYP/aug-ccpVTZ)						
	I	II	III	IV	V	VI	VII
r H-bond	189.4	222.3 246.7	183.1	185.7	234.1 259.8	–	199.5
r SiO$_2$	164.9	165.9	164.8	166.8	167.9	166.9	167.8
r SiO$_3$	167.2	166.5	166.4	164.8	166.0	166.4	166.1
r SiC$_4$	189.0	190.5	189.8	190.2	188.5	187.5	187.7
r SiC$_8$	187.0	186.4	187.0	187.1	186.6	186.9	186.6
r C$_6$O$_{20}$	122.5	122.7	122.5	122.6	121.7	121.7	122.0
r C$_6$N$_7$	135.8	135.4	135.7	135.6	137.2	134.4	135.8
∠OSiO	111.8	112.8	109.4	112.8	110.5	111.1	110.6
μ (Debye)	4.34	5.97	5.66	4.22	3.99	3.67	4.69
ΔE_0 (kcal mol^{-1})	0.00	0.99	1.27	1.90	4.03	3.48	4.40
	Water solution[a] (PCM-B3LYP/aug-ccpVTZ)						
	I	II	III	IV	V	VI	VII
r H-bond	175.0	211.9 242.8	172.9	173.6	231.0 332.3	–	191.4
r SiO$_2$	166.1	167.1	166.0	166.7	166.9	166.6	167.1
r SiO$_3$	166.9	167.3	166.5	166.0	166.4	166.5	166.1
r SiC$_4$	188.5	189.2	189.2	188.8	190.0	188.0	188.2
r SiC$_8$	187.0	186.5	186.9	187.2	186.8	186.9	186.7
r C$_6$O$_{20}$	124.2	124.1	124.2	124.2	123.5	123.5	123.7
r C$_6$N$_7$	133.9	133.8	133.8	133.8	134.6	134.5	134.2
∠OSiO	111.2	111.0	110.2	111.5	111.5	111.5	111.3
μ (Debye)	6.43	8.88	8.99	6.94	5.91	6.04	6.66
ΔE_0 (kcal mol^{-1})	1.65	5.57	1.87	2.29	3.05	0.00	2.39
E_0^{sol} (kcal mol^{-1})	**−17.91**	**−14.98**	**−18.95**	**−19.18**	**−20.54**	**−23.04**	**−21.57**

[a] Bond distances in pm

in solution are the decrease in the length of the intramolecular hydrogen bonds and the increase in the dipole moments.

Values of solvation energies indicate that all the structures are highly stabilized in water solution. As shown in Table 6, for DHSF gas phase and solution stability orders are inverted, being the so-called conformer VI the global minima in water solution. Likewise, the stability order in water solution of the set of conformers of DHSF differs from that calculated in gas-phase at the same level of theory. Those structures which are less stable in gas-phase are calculated to have the highest E_0^{sol}. Conformer VI is the global minima in solution and has the highest E_0^{sol} value. This observation supports the electrostatic explanation of the ring anomeric effect since. As it is known [42], increasingly polar solvents attenuate dipole-dipole interactions of polar bonds in the anomeric center, leading to a higher contribution of equatorial conformers in solution. Thus, under the PCM model, conformer III of DHSF becomes more stable than conformer II, and conformer I (which has two *axial* hydroxyl groups) has the highest relative energy value and the minor value of E_0^{sol} (solvation energy). For DHSP, conformers with *equatorial* arrangement of the *exo* - OH group are those with the highest contribution (more stable) in water solution, as is shown by their solvation energies.

Conclusions

1. The potential energy surfaces (PES) of two different gem-silanediols, namely DHSF and DHSP, have been analyzed at the B3LYP/6-31+G* level of theory, revealing the existence of six conformers for DHSF and seven for DHSP. Most of the structures are characterized for the occurrence of intramolecular hydrogen bonding between hydroxyl groups and adjacent aminocarbonyl groups, resulting in *pseudo*-cyclic structures. In some cases, more than one intramolecular H-bond is possible.

2. AIM analysis, NBO calculations and Rozenberg's enthalpy-distance relationship have been used to characterize and evaluate strength of individual hydrogen bonds in such systems. There exists a remarkable correlation between the calculated values of the $\nabla^2\rho(r)$ at each BCP, NBO orbital interaction energies and enthalpy values among the set of conformers considering those nine that present intramolecular hydrogen bonds.

3. The strength of the hydrogen bond and the magnitude of the ring and generalized anomeric effects have been put together in order to justify the stability order within each family of conformers. For DHSF, structures with stronger hydrogen bonds and higher magnitudes of the RAE and GAE are calculated to be more stable in gas phase. For DHSP such parallelism is not so straightforward, possibly due to the combined effect of the three stabilizing effects or the occurrence of additional destabilizing interactions,

such as steric effects, as the side chains are folded to establish H-bonds.

4. Solvent calculations were performed over the series of conformers to evaluate the influence of aqueous media in the structure and stability of the studied systems. For DHSF, stability order is totally inverted on going from gas-phase to water solution. Conformers with *equatorial* disposition of anomeric substituent are calculated to be more stable in solution which, in fact, is in accordance with the electrostatic explanation of RAE. For DHSP such stability inversion is not as symmetric as for DHSF, but those conformers with *equatorial* substituents are also estimated to be more stabilized than *axial* structures as evidenced by their E_0^{sol} values.

Supporting information available Potential energy surfaces of DHSF (Fig. S1) and DHSP (Fig. S2). Main geometrical parameters calculated at the MP2/cc-pVDZ level of theory for DHSF (Table S1) and DHSP (Table S2). NBO electronic populations calculated at the MP2/cc-pVDZ level of theory for DHSF (Table S3) and DHSP (Table S4).

References

1. Nguyen J-T, Hamada Y, Kimura T, Kiso Y (2008) Design of potent aspartic protease inhibitors to treat various diseases. Arch Pharm Chem Life Sci 341:523–535

2. Sieburth SMN, Chen C-A (2006) Silanediol protease inhibitors: from conception to validation. Eur J Org Chem 2:311–322, and references therein

3. Nielsen L, Skrydstrup T (2008) Sequential C−Si bond formations from diphenylsilane: application to silanediol peptide isostere precursors. J Am Chem Soc 130:13145–13151

4. Brinker CJ, Scherer GW (1989) Sol-Gel science: the physics and chemistry of Sol-Gel processing. Academic, San Diego

5. Ignatyev IS, Partal F, López González JJ (2004) Intramolecular hydrogen bonding in silanediols. J Mol Struct (THEOCHEM) 678:249–256

6. Sramko M, Vladimir G, Remko M (2008) Thermodynamics of binding of angiotensin-converting enzyme inhibitors to enzyme active site model. J Mol Struct (THEOCHEM) 869:19–28

7. Dedachi K, Khan MTH, Sylte I, Kurita N (2009) A combined simulation with ab initio MO and classical vibrational analysis on the specific interactions between thermolysin and dipeptide ligands. Chem Phys Lett 479:290–295

8. Dedachi K, Hirakawa T, Fujita S, Khan MTH, Sylte I, Kurita N (2011) Specific interactions and binding free energies between thermolysin and dipeptides: Molecular simulations combined with Ab initio molecular orbital and classical vibrational analysis. J Comput Chem 32:3047–3057

9. Hirakawa T, Fujita S, Ohyama T, Dedachi K, Khan MTH, Sylte I, Kurita (2012) Specific interactions and binding energies between thermolysin and potent inhibitors: molecular simulations based on ab initio molecular orbital method. J Mol Graph Model 33:1–11

10. Bader RFW (1990) Atoms in molecules. A quantum theory. Oxford University Press, New York

11. Reed AE, Curtiss LA, Weinhold F (1988) Intermolecular interactions from a natural bond orbital, donor-acceptor viewpoint. Chem Rev 88:899–926

12. Rozenberg M, Loewenschuss A, Marcus Y (2000) An empirical correlation between stretching vibration redshift and hydrogen bond length. Phys Chem Chem Phys 2:2699–2702

13. Frisch MJ et al. (2009) Gaussian 09, Revision B.01. Gaussian, Wallingford

14. Becke AD (1993) Density-functional thermochemistry. III. The role of exact exchange. J Chem Phys 98:5648–5652

15. Lee C, Yang W, Parr RG (1988) Development of the Colle-Salvetti conelation energy formula into a functional of the electron density. Phys Rev B 37:785–789

16. Zhao Y, Truhlar DG (2006) A new local density functional for main-group thermochemistry, transition metal bonding, thermochemical kinetics, and noncovalent interactions. J Chem Phys 125:194101

17. Binkley JS, Pople JA (1975) Møller–Plesset theory for atomic ground state energies. Int J Quantum Chem 9:229–236

18. Woon DE, Dunning TH (1993) Gaussian basis sets for use in corre-lated molecular calculations. III. The atoms aluminum through argon. J Chem Phys 98:1358–1371

19. Kendall RA, Dunning TH, Harrison RJ (1992) Electron affinities of the first-row atoms revisited. Systematic basis sets and wave func-tions. J Chem Phys 96:6796–6806

20. Zhao Y, Truhlar DG (2008) The M06 suite of density functionals for main group thermochemistry, thermochemical kinetics, noncovalent interactions, excited states, and transition elements: two new func-tionals and systematic testing of four M06-class functionals and 12 other functionals. Theor Chem Acc 120:215–241

21. Amin EA, Truhlar DG (2008) Zn coordination chemistry: develop-ment of benchmark suites for geometries, dipole moments, and bond dissociation energies and their use to test and validate density func-tionals and molecular orbital theory. J Chem Theory Comput 4:75–85

22. Grimme S, Antony J, Ehrlich S, Krieg H (2010) A consistent and accurate ab initio parametrization of density functional dispersion correction (DFT-D) for the 94 elements H-Pu. J Chem Phys 132:154104/1–154104/19

23. Cohen AJ, Mori-Sánchez P, Weitao Y (2012) Challenges for density functional theory. Chem Rev 112:289–320

24. Miertus S, Scrocco E, Tomasi J (1981) Approximate evaluations of the electrostatic free energy and internal energy changes in solution processes. Chem Phys 55:117–129

25. Carpenter JE, Weinhold F (1988) Analysis of the geometry of the hydroxymethyl radical by the "different hybrids for different spins" natural bond orbital procedure. J Mol Struct (Teocham) 169:41–62

26. Biegler-König F, Schönbohm J, Bayles D (2001) AIM2000 - a program to analyze and visualize atoms in molecules. J Comput Chem 22:545–559

27. Biegler-König F, Schönbohm J (2002) Update of the AIM2000-Program for atoms in molecules. J Comput Chem 23:1489–1494

28. Rodríguez PG, Montejo M, Marchal Ingraín A, Márquez F, López González JJ (2012) Dimethylsilanediol: structure and vibrational spectra by IR and Raman spectroscopies and quantum chemical calculations. Vib Spectrosc 58:79–86

29. Rodríguez PG, Montejo M, Marchal Ingraín A, Márquez F, López González JJ (2012) Synthesis and structural study of ethylmethyl-silanediol by quantum chemical calculations and IR and Raman spectroscopies. J Sol-Gel Sci Tech 61:258–267

30. Rodríguez PG, Montejo M, Marchal Ingraín A, Márquez F, López González JJ (2012) Molecular structure and vibrational spectra anal-ysis of diethylsilanediol by IR and Raman spectroscopies and DFT calculations. J Sol-Gel Sci Tech 64:54–62

31. Sobczyk L, Grabowski SJ, Krygowski TM (2005) Interrelation between H-Bond and Pi-Electron Delocalization. Chem Rev 105:3513–3560

32. Jabłoński M, Kaczmarek A, Sadlej AJ (2006) Estimates of the energy of intramolecular hydrogen bonds. J Phys Chem A 110:10890–10898, and references therein

33. Jabłoński M (2010) Full vs. constrain geometry optimization in the open–closed method in estimating the energy of intramolecular charge-inverted hydrogen bonds. Chem Phys 376:76–83, and references therein

34. Wendler K, Thar J, Zahn S, Kirchner B (2010) Estimating the hydrogen bond energy. J Phys Chem A 114:9529–9536, and refer-ences therein

35. Iogansen AV (1996) IR spectra and hydrogen bond energies of crystalline acid salts of carboxylic acids. Spectrochim Acta A 52:1559–1563

36. Koch U, Popelier PLA (1995) Characterization of C-H-O hydrogen bonds on the basis of the charge density. J Phys Chem 99:9747–9754

37. Thacher GRJ (1993) The anomeric effect and associated stereoelectronics effects. American Chemical Society Symposium Series, Washington, p 539

38. Kirby J (1983) The anomeric effect and related stereoelectronic effects at oxygen. Springer, New York

39. Lesarri A, Vega-Toribio A, Suenram RD, Brugh DJ, Nori-Shargh D, Boggs JE, Grabow J-U (2011) Structural evidence of anomeric effects in the anesthetic isoflurane. Phys Chem Chem Phys 13:6610–6618

40. Gorenstein DG (1987) Stereoelectronic effects in biomolecules. Chem Rev 87:1047–1077

41. Juaristi E, Cuevas G (1995) The Anomeric Effect. CRC, Boca Ratón

42. Eliel EL, Giza CA (1968) Conformational analysis. XVII. 2-Alkoxy- and 2-alkylthiotetrahydropyrans and 2-alkoxy-1,3-dioxanes. Anomeric effect. J Org Chem 33:3754–3758